



Magnetic field sensor based on helical long-period fiber grating with a three-core optical fiber

YUANYUAN ZHAO,¹ SHEN LIU,^{1,4}  CONG XIONG,¹ YING WANG,^{1,5} ZHENGYONG LI,¹ ZHONGYUAN SUN,^{1,2} JIANQING LI,³  AND YIPING WANG¹

¹Key Laboratory of Optoelectronic Devices and Systems of Ministry of Education/GuangDong Province, College of Physics and Optoelectronic Engineering, Shenzhen University, Shenzhen 518060, China

²Aston Institute of Photonic Technologies, Aston University, Birmingham, UK

³Guangdong-Hong Kong-Macao Joint Laboratory for Intelligent Micro-Nano Optoelectronic Technology, Macau University of Science and Technology, Avenida Wai Long, Taipa, Macau, China

⁴shenliu@szu.edu.cn

⁵yingwang@szu.edu.cn

Abstract: A high sensitivity optical fiber magnetic field sensor is proposed and implemented by using a helical long-period fiber grating (HLPFG) based on a three-core fiber (TCF) bonded to a U-shaped aluminum (Al) wire. An electrical current flowing through the Al wire in a perpendicular magnetic field can generate Ampere force, which changes the distance between the two arms of the U-shaped Al wire. Thus, when the intensity and direction of the magnetic field change, the bending curvature of TCF-HLPFG bonded to the U-shaped Al wire varies with the change of Ampere force, which is represented as the shift of resonant wavelength in the spectrum. The as-fabricated sensor can respond to the magnetic field direction and the intensity with a range from -15 mT to 15 mT, and the measured sensitivity is 456.5 pm/mT with Al wire electrical current 1 A. The proposed sensor has the advantages of low cost, nondestructive measurement method and ease manufacture, and is expected to be applied to weak magnetic field measurements.

© 2021 Optical Society of America under the terms of the [OSA Open Access Publishing Agreement](#)

1. Introduction

Magnetic field sensors have been widely used in military, medicine, general industry. Many electronic techniques for developing magnetic field sensors, including search coils, Hall-effect sensors, anisotropic magnetoresistive devices, and giant magnetoresistive devices, have been explored [1]. Compared with traditional methods, optical technology in magnetic field measurement present has obvious advantages such as low cost, low power consumption, the possibility of miniaturization, and immunity to electromagnetic interference and so on [2]. Optical magnetic field sensors based on Faraday effect [3], magneto-optic effect [4,5], magnetic-strict effect [6,7], magnetic force [8] or other mechanisms have been extensively studied. Among them, the feasibility of using Faraday effect for magnetic field sensing has been demonstrated in an all-fiber optical magnetic field sensor, but the sensor cannot directly respond to the direction of magnetic field, and the sensitivity of magnetic field is fairly low. Therefore, optical magnetic field sensors based on magneto-optic effect are widely studied to improve the magnetic field sensitivity [9]. The efficiency of magneto-optical effect is mainly determined by the materials, such as magnetic fluid (MF). MF is one of the most sensitive magneto-optical materials, which has the ability to quickly adjust its refractive index under the magnetic field [10,11]. In 2012, Gao et al. [4] reported a highly-sensitive magnetic sensor utilizing a D-shaped long-period fiber grating (LPG) immersed in an MF. Although the microfiber (several micrometers in diameter) exhibits a

higher sensitivity, it comes at the cost of reduced mechanical strength. For magnetic-strict effect, in 2009, Yang et al. [6] proposed using TbDyFe with magnetic-strict effect as a magneto-optic fiber for magnetic field sensing. However, the magnetic saturation and hysteresis inherent in magnetic materials may greatly reduce the dynamic range of material stretching, resulting in inaccurate sensor measurements. In addition, a novel Ampere force-based magnetic field sensor was reported, which circumvents saturation and hysteresis, but it cannot identify the direction of the magnetic field [12].

Bending sensors based on LPFGs have been demonstrated in different configurations. For example, in 2017, Wang et al. [13] proposed a two-dimensional bending sensor based on two non-orthogonal LPFGs in a three-core fiber (TCF). In 2014, Zhang et al. [14] developed a bending vector sensor consisting of a strong coupling LPFG and a slight-lateral-offset fusion splicing. The helical long-period fiber grating (HLPFG) has many of the same characteristics as ordinary LPFG, thus it can also be used as fiber bending sensor. For instance, in 2017, Cao et al. [15] presented a HLPFG with the periodic helical index modulation by twisting the double-clad fiber, and investigated its bending characteristics. In 2018, Li et al. [16] demonstrated a bending sensor based on single-mode fiber (SMF) HLPFG, achieving a sensitivity of 1.94 nm/(1/m).

In this letter, we propose a novel optical fiber vector magnetic field sensor based on a structure consist of a TCF-HLPFG and a U-shaped aluminum (Al) wire. When the current flows through the U-shaped Al wire, in a magnetic field perpendicular to the current, the two arms of the U-shaped Al wire will generate Ampere force, which will change the distance between the two arms of the U-shaped Al wires, thus leading to the change of bending curvature of TCF-HLPFG. Such a fiber-optic magnetic field sensor exhibits a high sensitivity of 456.5 pm/mT when Al wire electrical current is 1A. In addition, the sensor can also identify the direction of magnetic field by changing the direction of the Ampere force. To the best of our knowledge, this is the first time to realize magnetic field vector sensing by using HLPFG combined with magnetic force effect.

2. Sensor design and fabrication

In this experiment, a commercial TCF is used to fabricate the TCF-HLPFG. As shown in Fig. 1(a), the three cores are distributed along a line, and the distance between the two external cores and the central core is measured approximately 21.8 μm . The diameters of the center core and the two external cores are measured to be 8.3 and 7.6 μm , respectively. The cladding diameter of TCF is about 125 μm , which matches the diameter of a standard SMF.

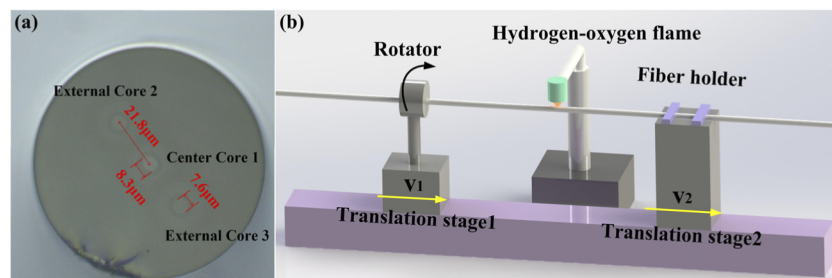


Fig. 1. (a) Microscopic image of the cross section of the TCF. (b) Schematic diagram of the TCF-HLPFG fabrication device.

A hydrogen-oxygen flame heating system, consisting of a rotation motor, hydrogen generator, and two translation stages, is employed to fabricate the TCF-HLPFG [17]. The schematic diagram of the simplified fabrication system is shown in Fig. 1(b). The two fiber holders are used to support the TCF, and the velocities of two translational stages and the rotate speed of the rotator are controlled by computer to adjust the diameter of the fiber and the pitch of HLPFG. In this

experiment, the velocities of the two translation stages are set as $v_1 = 0.8$ mm/s and $v_2 = 1.6$ mm/s, respectively. A schematic diagram of the proposed sensor is shown in Fig. 2(a). The length of TCF-HLPPFG is controlled to 15.5 mm, and both ends of the grating section are spliced with standard SMF. The microscopic image of a TCF-HLPPFG with 85 μm diameter and 480 μm grating pitch is shown in Fig. 2(b). The diameter of TCF is controlled using the relative velocity of two translational stages as the heated optical fiber is fused. The helical pitch of TCF-HLPPFG can be controlled by adjusting the rotate speed of the rotation motor [18]. The transmission spectrum of the fabricated sensor is characterized by connecting the two ends of the device to a broadband light source (BBS) (1250 to 1650 nm) and an optical spectrum analyzer (OSA, AQ6317B, ANDO) with 0.02 nm resolution. Figure 2(c) shown the transmission spectrum of the TCF-HLPPFG with a 1563.88 nm of resonant wavelength and 33.22 dB of transmission contrast. Here, the mode coupling behavior of the proposed TCF-HLPPFG is similar to that of the conventional LPPFG. The mode coupling between the fiber core and cladding modes of the proposed TCF-HLPPFG will occur when the following resonance condition is satisfied [15].

$$\lambda_i = (n_{core} - n_{cladding}^i)\Lambda \quad (1)$$

where n_{core} and $n_{cladding}^i$ are the effective refractive index of fundamental core mode and the i th order cladding mode respectively, Λ is the grating period, and λ_i is the i th order resonance wavelength.

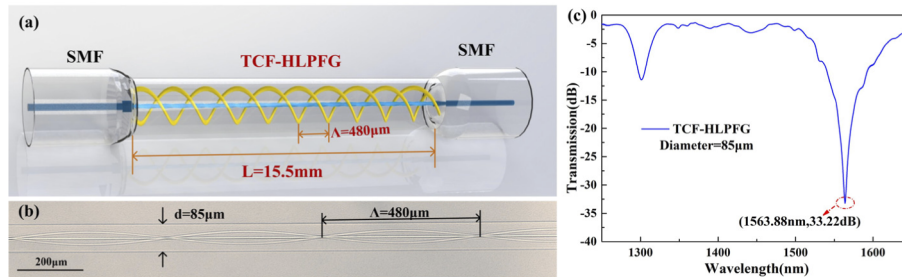


Fig. 2. (a) Schematic diagrams of the proposed sensor. (b) Microscopic image of the grating section. (c) Transmission spectrum of the TCF-HLPPFG

3. Sensitivity to magnetic field

A schematic diagram of the experimental setup used for magnetic field sensing is shown in Fig. 3(a). The magnetic field generator is formed by two electromagnets. The magnetic field intensity is adjusted by changing the magnitude of the supply current and calibrated by a gauss meter. In this experiment, the Al wire is designed into a U-shaped structure and connected with a power source and a resistance to form a loop. In this way, the value of current flowing through the two arms of the U-shaped wire is exactly the same, and the two arms of the U-shaped wire can generate the same amount of Ampere force. The direction of the Ampere force can be determined by the left-hand rule. Since the existence of the U-shape wire, the electrical currents flowing in the two arms are parallel to each other and in opposite directions. Then, the direction of the Ampere forces in the two arms are opposite in the same external magnetic field, resulting in a smaller distance between the two arms, i. e., increasing the bending curvature of the grating, as shown in Fig. 3(b). However, when the direction of the applied magnetic field is reversed, the direction of the Ampere forces in the two arms will also reverse accordingly, leading to a larger distance, i. e., decreasing the bending curvature of the grating, as shown in Fig. 3(c). The TCF-HLPPFG is placed vertically on the two arms of the U-shaped wire and the contact points

are fixed with UV glue. The BBS and OSA are used to detect a shift in transmission spectra wavelength of the TCF-HLPPFG during the experiment.

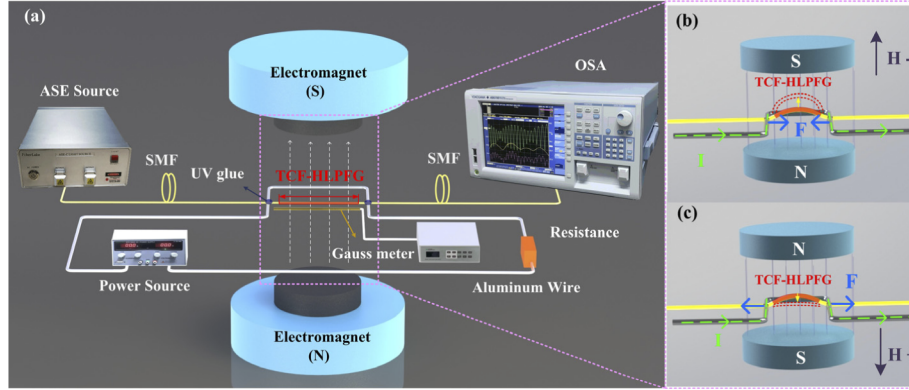


Fig. 3. (a) Experimental setup for magnetic field sensing. Schematic diagram of deformation of TCF-HLPPFG under negative (b) and positive (c) magnetic fields.

It is well known that the Ampere force generated by a current in a perpendicular magnetic field can be expressed as [12]

$$F_H = I \cdot H \cdot L_H \quad (2)$$

where F_H is the Ampere force, I is the electrical current, H is the magnitude of magnetic field, and L_H is the length of the wire carrying the current within the perpendicular magnetic field. It is worth mentioning that the TCF-HLPPFG is glued to the U-shaped Al wire and staying in an initial status of slightly bending curvature. When the two arms of the U-shaped structure are close to each other under the action of Ampere force, the bending curvature of the grating will further increase, resulting in the blue-shift of the resonant wavelength. On the contrary, when the direction of the applied magnetic field is reversed, the direction of the Ampere force will be reversed accordingly, leading to the red-shift of the resonant wavelength. Thus, the direction of the magnetic field can be identified through monitoring the shift direction of resonant wavelength of the TCF-HLPPFG. The change of curvature-induced δn_{eff} variation leads to the resonance wavelength shift. The theoretical resonance wavelength shift is obtained using the same approach as in [12,19]:

$$\Delta\lambda = \left[\frac{\lambda}{(\delta n_{eff} - \delta n_g)} \cdot \frac{d\delta n_{eff}}{dR} + \frac{(\delta n_{eff})^3}{\delta n_g} \cdot \frac{d\Delta}{dR} \right] \cdot \Delta R \quad (3)$$

where $\delta n_{eff} = n_{co\,eff} - n_{cl\,eff}$ is the differential effective index between the cladding mode and the core mode, $\delta n_g = n_{co\,g} - n_{cl\,g}$ is the differential group index, R is the curvature radius. The curvature-induced δn_{eff} variation plays a leading role in determining $\Delta\lambda$, which can be used to accurately detect the magnetic field by monitoring the change of the transmission spectra wavelength.

In this experiment, the Al wire current is fixed at 1A to detect the response of the sensor to magnetic field intensity. When the direction of the magnetic field is negative and the magnetic field intensity is increased from 0 to -30 mT with a step of 5 mT, the transmission spectra at different magnetic field intensity are illustrated in Fig. 4(a). The wavelength blueshifts from 1543.88 to 1521.01 nm with a total shift of 22.87 nm. When the direction of the magnetic field is positive and the magnetic field intensity is increased from 0 to 30 mT with a step of 5 mT, the transmission spectra at different magnetic field intensity are illustrated in Fig. 4(b). The results show that the resonance wavelength redshifts from 1543.88 nm to 1551.31 nm with total

shift of 7.43 nm. Moreover, the contrast of the transmission spectra varies with the increase of magnetic field intensity in the negative and positive directions, as shown in Figs. 4(a) and 4(b). This is because that the coupling energy of the core mode to the cladded mode is mainly dependent on the overlap of the two modes and the induced waveguide perturbation in the LPFG [20]. Figure 4(c) shows the relationship between the wavelength shift and magnetic field intensity along the positive and negative directions in the ± 30 mT range. The result shows that the shift of resonance wavelength is nonlinear with the variation of magnetic field intensity. A linear fitting method is used to characterize the sensitivity of the sensor to the magnetic field intensity. The linear response region appears from -15 to 15 mT, as shown in Fig. 4(d). The sensitivity of the wavelength shift is calculated to be 456.5 pm/mT when the Al wire electrical current is 1 A.

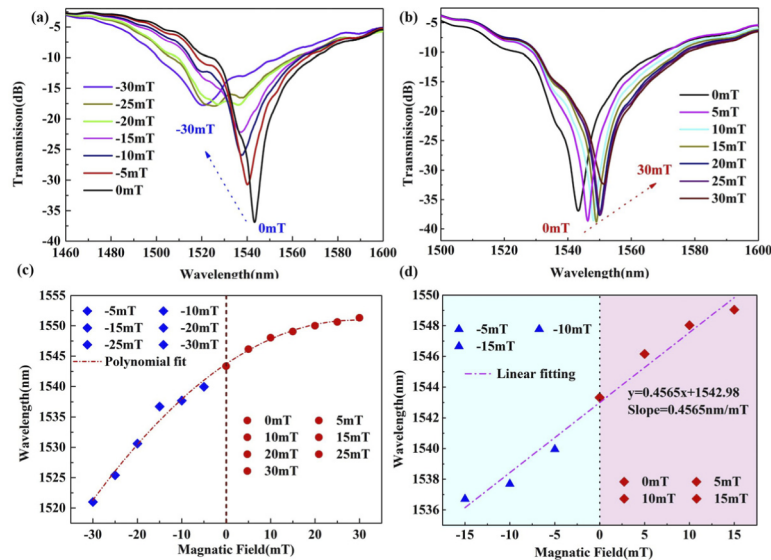


Fig. 4. Transmission spectra of the TCF-HLPFG at (a) 0 to -30 mT and (b) 0 to 30 mT of magnetic field intensity at 1 A Al wire current. (c) Non-linear relationship between the magnetic field intensity and resonant wavelength shift. (d) Linear part of the resonant wavelength shift.

There are two factors (electrical current I and magnetic field H) affect the characteristics of magnetic field sensor. To investigate the response of the sensor to electrical current, the magnetic field intensity is fixed at 50 mT, and then the value of electrical current is gradually increased. Figure 5(a) shows the transmission spectra of the TCF-HLPFG at different values of electrical current. The resonant wavelength shift and transmission contrast variation with electrical current increases are shown in Fig. 5(b). When the current increases from 0.9 A to 1.6 A, the wavelength shifts from 1546.80 to 1552.31 nm with a total shift of 5.51 nm, and the transmission contrast changes from -41.62 to -25.87 dB. The electrical current sensitivities are calculated by applying the linear fit to the experimental data, producing a 8.9 nm/A for the transmission wavelength demodulation and a 23 dB/A for the intensity demodulation, respectively. It can be speculated that the performance of this sensor can be improved by increasing the applied current.

In order to improve the sensitivity of the magnetic sensor based on TCF-HLPFG, as shown in Eq. (2), the Ampere force is proportional to the product value ($I \cdot H$) of the electrical current and the magnetic field intensity. Moreover, the data in Fig. 4(c) are recalculated and the relationship between the resonant wavelength and $I \cdot H$ is replotted, as shown in Fig. 6. Obviously, the wavelength shift is proportional to the product value ($I \cdot H$). Here, the Ampere force increases as the electrical current increasing while the magnetic applied remains constant, resulting in a

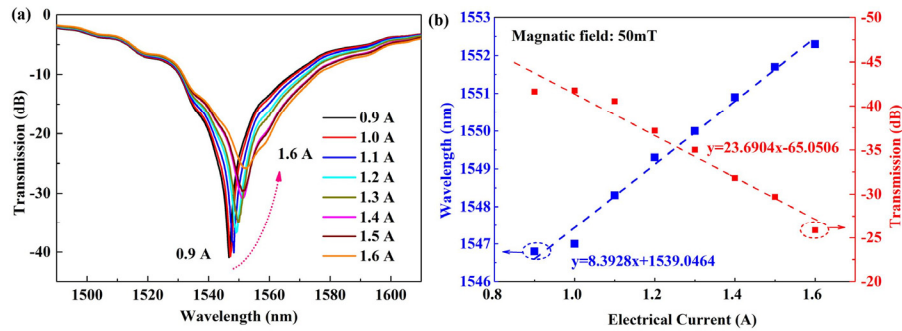


Fig. 5. (a) Transmission spectra of the TCF-HLPFG vary with the current at a magnetic field intensity of 50 mT. (b) Linear correlation between the resonance wavelength or grating contrast and the electric current.

larger resonant wavelength shift. Thus, the sensitivity of the magnetic sensor can be improved through applying a larger electrical current.

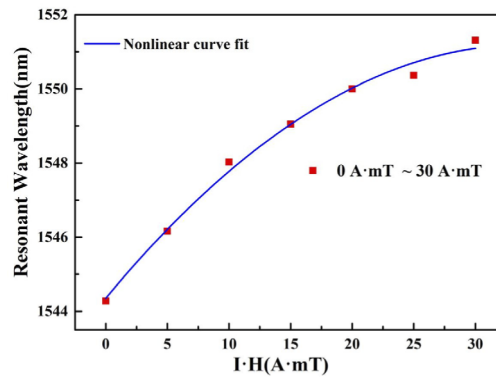


Fig. 6. The relationship between the resonant wavelength and $I \cdot H$.

For comparison, Table 1 exhibits the sensing performance of various optical fiber magnetic field sensors. The magnetic field intensity sensitivity of the sensor presented in this study is competitive with that of other sensors. More importantly, the magnetic field sensor bonded TCF-HLPFG to the U-shaped Al wire has a non-destructive surface topography and the ability to identify the magnetic field direction due to the curvature properties of HLPFG.

Table 1. Comparison of Magnetic Field Sensors with Different Sensing Performance.

Structure	Sensitivity	Range	Direction of discriminant
LPFG within a D-shaped [4]	176.4 pm/mT	1.4~189.7 mT	NO
Electroforming LPFG [21]	-0.465 dB/mT	0~47.6 mT	NO
MSM fiber sensor with MF-filled tube [22]	123 pm/mT	0.6~21.4 mT	NO
MZI with a MF component [23]	20.8 nm/mT	5~9.5 mT	NO
MF into a hollow-core waveguide [24]	292 pm/mT	0~30 mT	YES
Side-polished MMF [25]	6920 pm/mT	0~40 mT	YES
MF with SPF-SNS [26]	2370 pm/mT	2~6 mT	YES
TCF-HLPFG (our work)	456.5 pm/mT	-15~15 mT	YES

4. Conclusions

In summary, we demonstrated a novel magnetic field sensor bonded TCF-HLPFG to the U-shaped Al wire, with the ability of simultaneous sensing to the magnetic direction and intensity. At the Al wire current of 1A, the sensitivity of this magnetic field sensor is up to 456.5 pm/mT in the magnetic field intensity range of -15~15 mT, and it is possible to further improve the sensor performance by increasing the applied current of the U-shaped Al wire. Moreover, the magnetic field sensor can distinguish different magnetic field directions by the red and blue shifts of resonant wavelength. The proposed sensor avoids magnetic saturation and hysteresis, and presents all the advantages of optical fiber magnetic field sensors. It means that the proposed sensor can give the significant potential for a new generation of magnetic field optical sensors.

Funding. National Natural Science Foundation of China (61905164, 61905165); Guangdong Basic and Applied Basic Research Foundation (2021A1515011834, 2018KQNCX219); Shenzhen Science and Technology Innovation Program (RCBS20200714114922296, JCYJ20180507182058432); Guangdong International Science and Technology Cooperation Programme (2019A050510047); Research Fund of Guangdong-Hong Kong-Macao Joint Laboratory for Intelligent Micro-Nano Optoelectronic Technology (No. 2020B1212030010); Shenzhen University Foundation (2019104).

Disclosures. The authors declare no conflicts of interest.

Data availability. Data underlying the results presented in this paper are not publicly available at this time but may be obtained from the authors upon reasonable request.

References

1. J. E. Lenz, "A review of magnetic sensors," *Proc. IEEE* **78**(6), 973–989 (1990).
2. A. Layeghi, H. Latifi, and O. Frazao, "Magnetic field sensor based on nonadiabatic tapered optical fiber with magnetic fluid," *IEEE Photonics Technol. Lett.* **26**(19), 1904–1907 (2014).
3. L. Sun, S. Jiang, and J. R. Marciante, "All-fiber optical magnetic-field sensor based on Faraday rotation in highly terbium-doped fiber," *Opt. Express* **18**(6), 5407–5412 (2010).
4. L. Gao, T. Zhu, M. Deng, K. S. Chiang, X. K. Sun, X. P. Dong, and Y. S. Hou, "Long-Period fiber grating within D-shaped fiber using magnetic fluid for magnetic-field detection," *IEEE Photonics J.* **4**(6), 2095–2104 (2012).
5. R. Gao, Y. Jiang, and S. Abdelaziz, "All-fiber magnetic field sensors based on magnetic fluid-filled photonic crystal fibers," *Opt. Lett.* **38**(9), 1539–1541 (2013).
6. M. H. Yang, J. X. Dai, C. M. Zhou, and D. S. Jiang, "Optical fiber magnetic field sensors with TbDyFe magnetostrictive thin films as sensing materials," *Opt. Express* **17**(23), 20777–20782 (2009).
7. S. M. Quintero, C. Martelli, A. M. Braga, L. C. Valente, and C. C. Kato, "Magnetic field measurements based on Terfenol coated photonic crystal fibers," *Sensors* **11**(12), 11103–11111 (2011).
8. L. H. Cheng, Z. Z. Guo, J. H. Han, L. Jin, and B. O. Guan, "Ampere force based magnetic field sensor using dual-polarization fiber laser," *Opt. Express* **21**(11), 13419–13424 (2013).
9. M. Sedlar and L. Pust, "Preparation of cobalt doped nickel ferrite thin films on optical fibers by dip-coating technique," *Ceram. Int.* **21**(1), 21–27 (1995).
10. S. H. Dong, S. L. Pu, and H. T. Wang, "Magnetic field sensing based on magnetic-fluid-clad fiber-optic structure with taper-like and lateral-offset fusion splicing," *Opt. Express* **22**(16), 19108–19116 (2014).
11. Z. P. Jiang, J. L. Dong, S. Q. Hu, Y. X. Zhang, Y. F. Chen, Y. H. Luo, W. G. Zhu, W. T. Qiu, H. H. Lu, H. Y. Guan, Y. C. Zhong, J. H. Yu, J. Zhang, and Z. Chen, "High-sensitivity vector magnetic field sensor based on side-polished fiber plasmon and ferrofluid," *Opt. Lett.* **43**(19), 4743–4746 (2018).

12. S. J. Qiu, Q. Liu, F. Xu, and Y. Q. Lu, "Ampere force based photonic crystal fiber magnetic field sensor," *Sens. Actuators, A* **210**, 95–98 (2014).
13. S. Wang, W. G. Zhang, L. Chen, Y. X. Zhang, P. C. Geng, Y. S. Zhang, T. Y. Yan, L. Yu, W. Hu, and Y. P. Li, "Two-dimensional microbend sensor based on long-period fiber gratings in an isosceles triangle arrangement three-core fiber," *Opt. Lett.* **42**(23), 4938–4941 (2017).
14. S. S. Zhang, W. G. Zhang, P. C. Geng, and L. Wang, "A Mach–Zehnder interferometer constructed using lateral offset and a long period fiber grating for two-dimensional bending vector sensing," *J. Opt.* **16**(1), 015501 (2014).
15. X. B. Cao, D. D. Tian, Y. Q. Liu, L. Zhang, and T. Y. Wang, "Sensing characteristics of helical long-period gratings written in the double-clad fiber by CO₂ laser," *IEEE Sens. J.* **18**(18), 7481–7485 (2018).
16. Z. Li, S. Liu, Z. Bai, C. Fu, Y. Zhang, Z. Sun, X. Liu, and Y. Wang, "Residual-stress-induced helical long period fiber gratings for sensing applications," *Opt. Express* **26**(18), 24114–24123 (2018).
17. Y. Y. Zhao, S. Liu, J. X. Luo, Y. P. Chen, C. L. Fu, C. Xiong, Y. Wang, S. Y. Jing, Z. Y. Bai, C. R. Liao, and Y. P. Wang, "Torsion, Refractive Index, and Temperature Sensors Based on An Improved Helical Long Period Fiber Grating," *J. Lightwave Technol.* **38**(8), 2504–2510 (2020).
18. C. L. Fu, S. Liu, Z. Y. Bai, H. Jun, C. R. Liao, Y. Wang, Z. L. Li, Y. Zhang, K. M. Yang, B. Yu, and Y. P. Wang, "Orbital angular momentum mode converter based on helical long period fiber grating inscribed by hydrogen–oxygen flame," *J. Lightwave Technol.* **36**(9), 1683–1688 (2018).
19. T. Allsop, A. Gillooly, V. Mezentsev, T. Earthgowl-Gould, R. Neal, D. J. Webb, and I. Bennion, "Bending and orientational characteristics of long period gratings written in D-shaped optical fiber," *IEEE Trans. Instrument. Meas.* **53**(1), 130–135 (2004).
20. U. L. Block, V. Dangui, M. J. F. Digonnet, and M. M. Fejer, "Origin of apparent resonance mode splitting in bent long-period fiber gratings," *J. Lightwave Technol.* **24**(2), 1027–1034 (2006).
21. C. C. Chiang and Z. J. Chen, "A novel optical fiber magnetic sensor based on electroforming long-period fiber grating," *J. Lightwave Technol.* **32**(19), 3331–3336 (2014).
22. X. Q. Lei, Y. C. Xu, Y. T. Yu, and B. J. Peng, "Fiber in-line magnetic field sensor based on Mach-Zehnder interferometer integrated with magnetic fluid," *Optoelectron. Lett.* **15**(1), 43–47 (2019).
23. Z. Y. Li, C. R. Liao, J. Song, Y. Wang, F. Zhu, Y. P. Wang, and X. P. Dong, "Ultrasensitive magnetic field sensor based on an in-fiber Mach–Zehnder interferometer with a magnetic fluid component," *Photonics Res.* **4**(5), 197–201 (2016).
24. W. H. Wang, H. M. Zhang, B. Li, Z. Li, and Y. P. Miao, "Optical fiber magnetic field sensor based on birefringence in liquid core optical waveguide," *Opt. Fiber Technol.* **50**, 114–117 (2019).
25. Y. F. Chen, W. T. Sun, Y. X. Zhang, G. S. Liu, Y. H. Luo, J. L. Doug, Y. C. Zhong, W. G. Zhu, J. H. Yu, and Z. Chen, "Magnetic Nanoparticles Functionalized Few-Mode-Fiber-Based Plasmonic Vector Magnetometer," *Nanomaterials* **9**(5), 785 (2019).
26. Y. X. Li, S. L. Pu, Y. L. Zhao, R. Zhang, Z. X. Jia, J. L. Yao, Z. J. Hao, Z. X. Han, D. H. Li, and X. J. Li, "All-fiber-optic vector magnetic field sensor based on side-polished fiber and magnetic fluid," *Opt. Express* **27**(24), 35182–35188 (2019).